A NONLINEAR ELIMINATION PRECONDITIONED INEXACT NEWTON METHOD FOR HETEROGENEOUS HYPERELASTICITY

SHIHUA GONG* AND XIAO-CHUAN CAI†

Abstract. We propose and study a nonlinear elimination preconditioned inexact Newton method for the numerical simulation of diseased human arteries with a heterogeneous hyperelastic model. We assume the artery is made of layers of distinct tissues and also contains plaques. Traditional Newton methods often work well for smooth and homogeneous arteries, but suffer from slow or no convergence due to the heterogeneousness of diseased soft tissues and the quasi-incompressible condition. The proposed nonlinear elimination method adaptively finds a small number of equations causing the nonlinear stagnation and then eliminates them from the global nonlinear system. By using the theory of affine invariance of Newton's method, we provide insight about why the nonlinear elimination method can improve the convergence of Newton iterations. Our numerical results show that the combination of nonlinear elimination with an initial guess interpolated from a coarse level solution can lead to a uniform convergence for Newton iterations for this class of very difficult nonlinear problems.

Key words. Finite elements, nonlinearly preconditioned Newton method, hyperelasticity, arterial walls

AMS subject classifications. 65F08, 65N55, 65N22, 74S05

1. Introduction.

Nonlinearly preconditioned inexact Newton algorithms [7, 8, 12, 13] have been applied with significant success to solve difficult nonlinear problems in computational fluid dynamic involving boundary layers, local singularities or shock waves. In this paper, we consider applying the nonlinearly preconditioning techniques to solve a heterogeneous hyperelastic problem of diseased arteries. Arterial walls are composed of three distinct tissue layers from inside to outside: the intima, the media, and the adventitia. The mechanical properties of the intima can be negligible. The other two layers can be modeled as fiber-enforced materials composed of nearly incompressible matrix substance with embedded collagen fibers. For the disease of atherosclerosis, some plaque components of calcification and lipids may build up inside the arteries. In [6], the authors consider several material models for diseased arterial walls in order to study the mechanical response and the influence on the nonlinear iterations. It is reported that the heterogeneousness of diseased soft tissues and the quasi-incompressible condition have negative effects on the convergence of Newtons iteration.

Nonlinear preconditioning can be applied on the left or on the right of the nonlinear function. The additive Schwarz preconditioned inexact Newton algorithm (ASPIN) [7] is an example of the left preconditioning, which changes the function of the system to a more balanced system. On the other hand, the right preconditioning such as the nonlinear elimination algorithm (NE) [8, 12, 13, 15] is applied by modifying the variables of the nonlinear function. NE is easier to implement than ASPIN since the nonlinear function does not have to be replaced. Moreover, more efficient and sophisticated linear solvers can be applied to the unchanged Jacobian.

However, a straightforward application of NE to hyperelasticity does not work well. Because it introduces sharp jumps in the residual function near the boundary

*Beijing International Center for Mathematical Research, Peking University, Beijing 100871, P. R. China.

†Department of Computer Science, University of Colorado Boulder, Boulder, CO 80309, USA, (cai@cs.colorado.edu).

of the eliminating subdomains. We refer to this as the thrashing phenomenon. Such jumps deteriorate the performance of nonlinear precondition. To resort this problem, we use the theory of affine invariance [10] to analyze the convergence of the damped Newton method with exact nonlinear elimination, and then provide some insight about how to design the nonlinear elimination preconditioner. Our proposed algorithm is a two-level method with two key components: an adaptive nonlinear elimination scheme and a nodal-value interpolation operator. The interpolation operator provides an initial guess with a coarse level approximation to deal with the global nonlinearity. Note that, for quasi-incompressible linear elasticity, the nodal interpolation is unstable since it does not preserve the volume. Thus, inexact Newton method fails even with the initial guess interpolated from a coarse level solution. With the help of adaptive nonlinear elimination scheme, we can capture the local pollution causing unbalanced nonlinearity and then eliminates it from the global system. We numerically show that this combination leads to a uniform convergence for Newton iterations.

The rest of paper is organized as follows. We present the model and the discretization for arterial walls in Section 2. The nonlinear elimination preconditioned Newton's method is proposed and discussed in Section 3. In Section 4, some numerical experiments are presented to demonstrate the performance of the nonlinear elimination preconditioning. The concluding remarks are given in the last section.

2. Model and discretization. We consider a hyperelastic model for arterial walls and its finite element discretization. First, we introduce some basic notations in continuum mechanics. The body of interest in the reference configuration is denoted by $\Omega \in \mathbb{R}^3$, parameterized by X, and the current configuration by $\tilde{\Omega} \in \mathbb{R}^3$, parametrized by x. The deformation map $\phi(X) = X + u : \Omega \mapsto \tilde{\Omega}$ is a differential isomorphism between the reference and current configuration. Here u is the displacement defined on the reference configuration. The deformation gradient F is defined by $\boldsymbol{F}(X) = \nabla\phi(X) = \boldsymbol{I} + \nabla u$, with the Jacobian $J(X) = \det \boldsymbol{F}(X) > 0$. The right Cauchy-Green tensor is defined by $\boldsymbol{C} = \boldsymbol{F}^T\boldsymbol{F}$. The hyperelastic materials postulate the existence of an energy density function ψ defined per unit reference volume. By the principle of material frame indifference[14], one can prove that the energy function is a function of $\boldsymbol{C}$, i.e., $\psi = \hat{\psi}(\boldsymbol{C})$. Based on a specific form of the energy function, the first and second Piola-Kirchhoff stress tensor are $\boldsymbol{P} = \boldsymbol{F}\boldsymbol{S}$ and $\boldsymbol{S} = 2\frac{\partial\psi}{\partial\boldsymbol{C}}$. And the Cauchy stress is given by $\boldsymbol{\sigma} = J^{-1}\boldsymbol{F}\boldsymbol{S}\boldsymbol{F}^T$. The balance of the momentum is governed by the following hyperelastic equation

$$\begin{cases} -\mathrm{div}(\boldsymbol{F}\boldsymbol{S}) = f, & \text{on } \Omega \\ u = \bar{u}, & \text{on } \Gamma_g, \\ \boldsymbol{P}N = \bar{t}, & \text{on } \Gamma_h, \end{cases} \tag{2.1}$$

where f is the body force vector, N denotes unit exterior normal to the boundary surface Γ_h and $\partial\Omega = \Gamma_g \cup \Gamma_h$ with $\Gamma_g \cap \Gamma_h = \emptyset$. In the rest of the paper, we always consider homogeneous Dirichlet boundary condition $\bar{u} = 0$ and the situation where the deformation is driven by external applied pressure load. The simple pressure boundary condition is a distributed load normal to the applied surface in the reference configuration; reads as $\bar{t} = -pN$. We are also interested in the follower pressure load [5], which is applied to the current deformed state; reads as

$$\bar{t} = -p(\mathrm{cof}\boldsymbol{F})N.$$

Here $\mathrm{cof}\boldsymbol{F} = J\boldsymbol{F}^{-T}$. is the cofactor of $\boldsymbol{F}$. It concerns the change in direction of the normals as well as the area change. The dependence on the deformed geometry makes

this a nonlinear boundary condition, which brings extra challenge for the convergence of the nonlinear solvers.

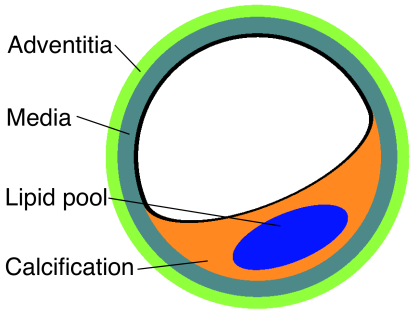

Fig. 2.1: Schematic cross-section of a diseased artery with two plaque components

2.1. Energy functions for arterial walls with plaques. We are interested in a diseased artery with two layers and two plaque components. The schematic cross-section of the artery is presented in Fig. 2.1. There are a calcification and a lipid pool. The adventitia and the media are modeled by a polyconvex energy function [4],

$$\psi_A = c_1\left(\frac{I_1}{I_3^{1/3}} - 3\right) + \epsilon_1\left(I_3^{\epsilon_2} + \frac{1}{I_3^{\epsilon_2}} - 2\right) + \sum_{i=1}^{2}\alpha_1\left\langle I_1 J_4^{(i)} - J_5^{(i)} - 2\right\rangle^{\alpha_2}. \tag{2.2}$$

Here, $\langle b\rangle$ denotes the Macaulay brackets defined by $\langle b\rangle = (|b|+b)/2$, with $b \in R$. And I_1, I_2, I_3 are the principal invariants of $\boldsymbol{C}$; i.e. $I_1 := \mathrm{tr}(\boldsymbol{C}), I_2 := \mathrm{tr}(\mathrm{cof}\boldsymbol{C}), I_3 := \det \boldsymbol{C}$. The additional mixed invariants $J_4^{(i)}, J_5^{(i)}$ characterize the anisotropic behavior of arterial wall and are defined as $J_4^{(i)} = \mathrm{tr}[\boldsymbol{C}\boldsymbol{M}^{(i)}], J_5^{(i)} := \mathrm{tr}[\boldsymbol{C}^2\boldsymbol{M}^{(i)}]$, for $i = 1:2$, where $\boldsymbol{M}^{(i)} := a^{(i)} \otimes a^{(i)}, i = 1, 2$ are the structural tensors with $a^{(i)}, i = 1, 2$ denoting the direction fields of the embedded collagen fibers. The polyconvexity condition in the sense of [2] is the essential condition to ensure the existence of energy minimizers and material stability.

Following [6], the lipid is modeled by the isotropic part of ψ_A used for the adventitia and media. The calcification area is modeled as isotropic Mooney-Rivlin material with the following energy function

$$\psi_C = \beta_1 I_1 + \eta_1 I_2 + \delta_1 I_3 - \delta_2 \ln I_3.$$

The model parameters of all the above energy functions are listed in Table 2.1.

Comp.	c_1[kPa]	ϵ_1[kPa]	ϵ_2[-]	α_1[kPa]	α_2	β_1[kPa]	η_1[kPa]	δ_1[kPa]	δ_2[kPa]
Adv.	6.6	23.9	10	1503.0	6.3	–	–	–	–
Med.	17.5	499.8	2.4	30001.9	5.1	–	–	–	–
Liq.	17.5	499.8	2.4	–	–	–	–	–	–
Cal.	–	–	–	–	–	80.0	250.0	2000.0	2580.0

Table 2.1: model parameters [6] of the energy functions

2.2. Finite element discretization. As reported in [3], the lowest-order Lagrange finite element with linear shape functions is not sufficient to provide a good approximation for the arterial wall stresses. We use the $\mathcal{P}_2$ Lagrange finite element to approximate the displacement. Let $V_0 \subset H_0^1(\Omega, \mathbb{R}^3)$ be the finite element space defined on Ω. The variational problem finds a solution $u \in V_0$ such that

$$a(u, v) := \int_\Omega \boldsymbol{F}\boldsymbol{S} : \nabla v \; dX + \int_{\Gamma_h} pJ\boldsymbol{F}^{-T} N \cdot v \; ds = \int_\Omega f \cdot v \; dX \quad \forall v \in V_0. \tag{2.3}$$

Here the subscript of V_0 indicates that the functions in V_0 vanish on Γ_g. Newton-type methods require the Jacobian form of $a(u, v)$, i.e.,

$$\begin{aligned} \delta a(u; \delta u, v) = &\int_\Omega \boldsymbol{F}^T \nabla \delta u : \mathbb{C} : \boldsymbol{F}^T \nabla v + \nabla \delta u \boldsymbol{S} : \nabla v \; dX \\ &+ \int_{\Gamma_h} pJ \left(\mathrm{tr}(\boldsymbol{F}^{-1} \nabla \delta u) I - \boldsymbol{F}^{-T} (\nabla \delta u)^T \right) \boldsymbol{F}^{-T} N \cdot v \; ds \end{aligned} \tag{2.4}$$

where $\mathbb{C} = \frac{\partial S}{\partial C} = \frac{\partial^2 \psi}{\partial C \partial C}$ is the material tangential moduli. An explicit formula to compute $\mathbb{C}$ for the general form of free energy can be found in [17].

3. Inexact Newton method with nonlinear elimination preconditioning. In this section, we first describe the motivation of nonlinear preconditioning based on an affine invariant convergence theorem of Newton-type methods. After that, we analyze the precondtioning effect of nonlinear elimination and then give a detailed description of the nonlinear elimination preconditioned inexact Newton method (NEPIN). We rewrite (2.3) as a system of n equations

$$F(u^*) = 0, \tag{3.1}$$

where $F \in C^1(D), F : D \mapsto \mathrm{R}^n$ with an n by n Jacobian $J = F'(u)$ and $D \subset \mathrm{R}^n$ open and convex. Given an initial guess u^0 of a solution u^*, the damped Newton method finds a sequence of iterates $\{u^k\}$ computed through

$$F'(u^k)p^k = -F(u^k), \quad u^{k+1} = u^k + \lambda^k p^k, \quad \lambda^k \in (0, 1] \tag{3.2}$$

Here p^k is the Newton direction and λ^k is a scalar determined by a monotonicity test:

$$T(u^{k+1}) \leq \theta T(u^k), \tag{3.3}$$

where $\theta \in (0, 1)$ and $T(u)$ is a level function measuring how close u is to the solution u^*. In most cases, one sets $T(u) = \frac{1}{2}\|F(u)\|^2$.

The convergence of $\{u^k\}$ to u^* is quadratic if the initial guess is close enough to the desired solution and $\lambda^k \to 1$. However, a good initial guess is generally unavailable and the monotonicity test (3.3) often results in a really small step length λ^k. This phenomenon is described rigorously in the following theorem under the framework of affine invariance [10] with a localized version of the affine contravariant Lipschitz condition:

Assumption 1. *The affine contravariant Lipschitz condition holds,*

$$\| \left(F'(u + \lambda p) - F'(u)\right) p \| \leq \omega_{F,u,\lambda} \lambda \|F'(u)p\|^2, \quad \textit{for any } u \in D. \tag{3.4}$$

Here p is the Newton direction of F at u and $\lambda \in (0, 1]$ such that $u + \lambda p \in D$. We assume $u + p \in D$ and let $\omega_{F,u} = \sup_{\lambda \in (0,1]} \omega_{F,u,\lambda}$. We also denote the global affine contravariant Lipschitz constant by $\omega_F = \sup_{u \in D} \omega_{F,u}$.

THEOREM 3.1. *Let $F'(u)$ be nonsingular for all $u \in D$ and Assumption 1 holds. With the notation $h_k := \omega_{F,u^k}\|F(u^k)\|$, and $\lambda \in [0, min(1, 2/h_k)]$, we have:*

$$\|F(u^k + \lambda p^k)\| \leq t_k(\lambda)\|F(u^k)\|, \tag{3.5}$$

where $t_k(\lambda) := 1 - \lambda + \frac{1}{2}\lambda^2 h_k$. Moreover, if $h_k < 2$, we have

$$\|F(u^k + p^k)\| \leq \frac{1}{2}\omega_F\|F(u^k)\|^2. \tag{3.6}$$

Proof. The proof here is presented for the completeness; see [10] for an original one. By applying Newton-Leibniz formula and Assumption 1, we obtain the estimate (3.5):

$$\begin{aligned}
\|F(u^k + \lambda p^k)\| &= \|F(u^k) + \int_{t=0}^{\lambda} F'(u^k + tp)p \; dt\| \\
&= \|(1-\lambda)F(u^k) + \int_{t=0}^{\lambda} \left(F'(u^k + tp^k) - F'(u^k)\right) p^k \; dt\| \\
&\leq \|(1-\lambda)F(u^k)\| + \int_{t=0}^{\lambda} t\omega_{F,u^k}\|F(u^k)\|^2 \; dt \\
&= (1 - \lambda + \frac{1}{2}\lambda^2 h_k)\|F(u^k)\|
\end{aligned}$$

To get a reduction on the norm of residual, the step length should be chosen in the interval $(0, min(1, 2/h_k)]$. Moreover, if $h_k \leq 2$, let $\lambda = 1$ and then we obtain the quadratic convergence (3.6). ∎

According to the theorem, the convergence is quadratic when $h_k < 2$. For $h_k \geq 2$, the optimal reduction rate of the residual, i.e. the minimal value of $t_k(\lambda)$ in (3.5), is $\bar{t}_k := 1 - \frac{1}{2h_k}$. The stagnation in the nonlinear residual curve appears if h_k is large. Thus, an intuitive idea to precondition Newton's method is to make the quantity

$$h_k := \omega_{F,u^k}\|F(u^k)\| \tag{3.7}$$

smaller. In the following, we transform the nonlinear function $F(u)$ to $\mathcal{F}(\tilde{u})$ via nonlinear elimination. Under appropriate assumptions, we prove that the local affine contravariant Lipschitz constant $\omega_{\mathcal{F},\tilde{u}^k,\lambda}$ of $\mathcal{F}$ as well as the new residual $\|\mathcal{F}(\tilde{u}^k)\|$ is smaller than that of the original nonlinear function F.

3.1. Exact nonlinear elimination. Assume $F(u)$ is partitioned as

$$F(u) = \begin{bmatrix} F_1(u_1, u_2) \\ F_2(u_1, u_2) \end{bmatrix}, \tag{3.8}$$

and $u = (u_1, u_2)^T$. For any u_2 in a projection set $D_2 = \{u_2 \mid (u_1, u_2)^T \in D\}$, we assume that there is an implicitly defined function $g(u_2)$ such that

$$F_1(g(u_2), u_2) = 0. \tag{3.9}$$

Then our preconditioned nonlinear problem reads as: finding u_2 such that

$$\mathcal{F}(u_2) := F_2(g(u_2), u_2) = 0. \tag{3.10}$$

We call $\bar{u} = (g(u_2), u_2)$ as the *cut-extension* of u_2. Next, we analyze the convergence of Newton's method applied to the preconditioned system. To derive the Jacobian of $\mathcal{F}$, consider the partitioned block Jacobian

$$J := F'(u) = \begin{bmatrix} J_{11} & J_{12} \\ J_{21} & J_{22} \end{bmatrix}, \tag{3.11}$$

where $J_{ij} = \frac{\partial F_i}{\partial u_j}$. Differentiating (3.9) as a function of u_2 leads to $J_{11}g'(u_2) + J_{12} = 0$, and if J_{11} is nonsingular, then $g'(u_2) = -J_{11}^{-1}J_{12}$. Then, by differentiating (3.10) and using the formula, we have

$$\mathcal{J}(u_2) := \mathcal{F}'(u_2) = (J_{22} - J_{21}J_{11}^{-1}J_{12})(g(u_2), u_2). \tag{3.12}$$

Note that $\mathcal{J}(u_2)$ is the Schur complement of $J(\bar{u})$, where $\bar{u} = (g(u_2), u_2)$ is the cut-extension of u_2. Let $p_2 := -\mathcal{J}^{-1}(u_2)\mathcal{F}(u_2)$ be the Newton direction of $\mathcal{F}$. We define a harmonic extension of p_2 by $p = (h(p_2), p_2)^T$ such that

$$J_{11}(\bar{u})h(p_2) + J_{12}(\bar{u})p_2 = 0,$$

or equivalently $h(p_2) = g'(u_2)p_2$. One can show that p actually is the Newton direction of F at $\bar{u}$ since

$$J(\bar{u})p = \begin{bmatrix} 0 \\ \mathcal{J}(u_2)p_2 \end{bmatrix} = \begin{bmatrix} -F_1\left(g(u_2), u_2\right) \\ -F_2\left(g(u_2), u_2\right) \end{bmatrix} = -F(\bar{u}).$$

Thus, we can obtain the precondtioned Newton direction p_2 directly by solving the original Jacobian system $J(\bar{u})p = -F(\bar{u})$ without assembling the Schur complement $\mathcal{J}(u_2)$. Moreover, we have the linear approximation property for sufficiently small λ

$$g(u_2 + \lambda p_2) \approx g(u_2) + g'(u_2)\lambda p_2 = g(u_2) + \lambda h(p_2).$$

Next we make an assumption, with which the preconditioning effect of $\mathcal{F}$ is proved.

ASSUMPTION 2. *For any $u \in D$, $J_{11}(u)$ is nonsingular and $\|J_{21}(u)J_{11}^{-1}(u)\|_1 \leq 1$.*

LEMMA 3.2. *If Assumption 2 holds, then for any $u = (u_1, u_2)^T \in D$, we have*

$$\|\mathcal{F}(u_2)\|_1 \leq \|F_2(u_1, u_2)\|_1 + \|J_{21}J_{11}^{-1}\|_1\|F_1(u_1, u_2)\|_1 \leq \|F(u_1, u_2)\|_1. \tag{3.13}$$

Proof. By Taylor expansion, we have

$$\begin{bmatrix} F_1(g(u_2), u_2) \\ F_2(g(u_2), u_2) \end{bmatrix} = \begin{bmatrix} F_1(u_1, u_2) \\ F_2(u_1, u_2) \end{bmatrix} + \begin{bmatrix} J_{11}(u_1^\theta, u_2)(g(u_2) - u_1) \\ J_{21}(u_1^\theta, u_2)(g(u_2) - u_1) \end{bmatrix}$$

where $u_1^\theta, u_1, g(u_2)$ are colinear. Since $F_1(g(u_2), u_2) = 0$ and J_{11} is nonsingular, we have $g(u_2) - u_1 = -J_{11}^{-1}F_1(u_1, u_2)$. Thus,

$$\mathcal{F}(u_2) = F_2(u_1, u_2) - (J_{21}J_{11}^{-1})(u_1^\theta, u_2)F_1(u_1, u_2).$$

By Assumption 2, we have $\|J_{21}J_{11}^{-1}\|_1 \leq 1$. (3.13) follows from the triangle inequality

$$\|\mathcal{F}(u_2)\|_1 \leq \|F_2(u_1, u_2)\|_1 + \|J_{21}J_{11}^{-1}F_1(u_1, u_2)\|_1 \leq \|F(u_1, u_2)\|_1.$$

LEMMA 3.3. *If Assumption 2 holds, then for any $u_2 \in D_2$, we have*

$$\frac{\|(\mathcal{J}(u_2+\lambda p_2)-\mathcal{J}(u_2))p_2\|_1}{\lambda\|\mathcal{J}(u_2)p_2\|_1^2} \le \frac{\|\left(J(\bar{v})-J(\bar{u})\right)p\|_1}{\lambda\|J(\bar{u})p\|_1^2}. \tag{3.14}$$

Here $p_2 := -\mathcal{J}^{-1}(u_2)\mathcal{F}(u_2), p := -J^{-1}(\bar{u})F(\bar{u}), \bar{v} := (g(u_2+\lambda p_2), u_2+\lambda p_2)$, and $\bar{u} := (g(u_2), u_2)$.

Proof. By a direct calculation, we have

$$\|\mathcal{J}(u_2)p_2\|_1 = \|J^{\bar{u}}p\|_1, \tag{3.15}$$

since $F_1(g(u_2), u_2) = 0$. Here we use the superscript $\bar{u}$ to indicate that the Jacobian is evaluated at $\bar{u}$, i.e. $J^{\bar{u}} = J(g(u_2), u_2)$. Set $\bar{v} = (g(u_2+\lambda p_2), u_2+\lambda p_2)^T$ and $v_2 = u_2 + \lambda p_2$. We have

$$\begin{aligned}
\|\left(J^{\bar{v}}-J^{\bar{u}}\right)p\|_1 &= \left\| \begin{bmatrix} J_{11}^{\bar{v}}h(p_2)+J_{12}^{\bar{v}}p_2 \\ J_{21}^{\bar{v}}h(p_2)+J_{22}^{\bar{v}}p_2 \end{bmatrix} - \begin{bmatrix} 0 \\ \mathcal{J}(u_2)p_2 \end{bmatrix} \right\|_1 \\
&= \left\| \begin{bmatrix} \left(-J_{11}^{\bar{v}}(J_{11}^{\bar{u}})^{-1}J_{12}^{\bar{u}}+J_{12}^{\bar{v}}\right)p_2 \\ \left(-J_{21}^{\bar{v}}(J_{11}^{\bar{u}})^{-1}J_{12}^{\bar{u}}+J_{22}^{\bar{v}}\right)p_2 \end{bmatrix} - \begin{bmatrix} 0 \\ \mathcal{J}(u_2)p_2 \end{bmatrix} \right\|_1 \\
&= \left\| \begin{bmatrix} \tilde{J}_{12}p_2 \\ J_{21}^{\bar{v}}(J_{11}^{\bar{v}})^{-1}\tilde{J}_{12}p_2 \end{bmatrix} + \begin{bmatrix} 0 \\ \left(\mathcal{J}(v_2)-\mathcal{J}(u_2)\right)p_2 \end{bmatrix} \right\|_1 \\
&= \|\tilde{J}_{12}p_2\|_1 + \|J_{21}^{\bar{v}}(J_{11}^{\bar{v}})^{-1}\tilde{J}_{12}p_2 + \left(\mathcal{J}(v_2)-\mathcal{J}(u_2)\right)p_2\|_1 \\
&\ge \|\left(\mathcal{J}(v_2)-\mathcal{J}(u_2)\right)p_2\|_1 + \left(1-\|J_{21}^{\bar{v}}(J_{11}^{\bar{v}})^{-1}\|_1\right)\|\tilde{J}_{12}p_2\|_1
\end{aligned} \tag{3.16}$$

where $\tilde{J}_{12} = -J_{11}^{\bar{v}}(J_{11}^{\bar{u}})^{-1}J_{12}^{\bar{u}} + J_{12}^{\bar{v}}$. Assumption 2 asserts $1-\|J_{21}^{v}(J_{11}^{v})^{-1}\| \ge 0$. Thus,

$$\|\left(\mathcal{J}(u_2+\lambda p_2)-\mathcal{J}(u_2)\right)p_2\|_1 \le \|\left(J^{\bar{v}}-J^{\bar{u}}\right)p\|_1. \tag{3.17}$$

∎

By (3.15) and (3.17), we complete the proof.

The analysis provides us some insight about how to design the nonlinear elimination preconditioner:

1. *The nonlinearly preconditioning effect* The convergence of Newton-type methods relies on a certain form of Lipschitz condition. In (3.4) of Lemma 3.3, the left-hand side is a characterization of the affine contravariant Lipschitz constant of $\mathcal{F}$. Whereas, for the right-hand side of F, it is not valid since the cut-extension

$$\bar{v} := \begin{pmatrix} g(u_2+\lambda p_2) \\ u_2+\lambda p_2 \end{pmatrix} \ne \bar{u}+\lambda p = \begin{pmatrix} g(u_2)+\lambda h(p_2) \\ u_2+\lambda p_2 \end{pmatrix}.$$

   However, we have $g(u_2+\lambda p_2) = g(u_2)+\lambda h(p_2)+\mathcal{O}(\lambda^2)$ and then $\bar{v} \approx \bar{u}+\lambda p$. Thus, let F be sufficiently smooth and by Lemma 3.3, we obtain, for small λ,

$$\omega_{\mathcal{F},u_2,\lambda} \le \omega_{F,\bar{u},\lambda} + \mathcal{O}(\lambda).$$

   If the stagnation in the nonlinear residual appears, Theorem 3.1 tells us that the optimal step length $\bar{\lambda}^k = \frac{1}{h_k}$ is really small. In such situations, the nonlinear elimination accelerates the convergence of Newton iteration by making the residual and the local affine contravariant Lipschitz constant smaller.

2. *How to perform nonlinear elimination* To apply a Newton step to the nonlinear elimination precondtioned system (3.10), one requires a solve of the Schur complement system
$$\mathcal{J}p_2 = \mathcal{F}$$
and several solves of $g(u_2 + \lambda p_2)$ during the line search step to satisfy
$$\|\mathcal{F}(g(u_2 + \lambda p_2), u_2 + \lambda p_2)\| \leq \theta \|\mathcal{F}(g(u_2), u_2)\|.$$
This is often considered too expensive in realistic applications. Fortunately, according to our analysis, we can obtain the precondtioned Newton direction p_2 directly by solving the original Jacobian system
$$J(\bar{u})p = -F(\bar{u}),$$
provided that $F_1(\bar{u}) = F_1(g(u_2), u_2) = 0$. And then we have $p = (h(p_2), p_2)$. Moreover, we have the approximation $(g(u_2 + \lambda p_2), u_2 + \lambda p_2) \approx \bar{u} + \lambda p$. Thus, the line search can be carried out approximately as
$$\|F(\bar{u} + \lambda p)\| \leq \theta \|F(\bar{u})\|.$$
From this point of view, the nonlinear elimination preconditioner only needs to update the approximate solution $u = (u_1, u_2)$ to $\bar{u} = (g(u_2), u_2)$ before each Newton iteration of the original problem, and the implementation of the Newton iteration does not change, including the assembling of the Jacobian and the linear solver.
3. *How to choose the eliminated equations* According to Lemma 3.2, the reduction rate on the residual is bounded by
$$\frac{\|F_2\|_1 + \|J_{21}J_{11}^{-1}\|_1 \|F_1\|_1}{\|F\|_1}.$$
To minimize the reduction rate, one should choose the eliminated equations F_1 with large residual components.
4. *How to choose the eliminated variables* Assumption 2 asserts $\|J_{21}J_{11}^{-1}\|_1 \leq 1$. A weaker requirement is
$$\|J_{21}(u)\|_1 \leq \|J_{11}(u)\|_1.$$
For some elliptic problems, it is usually satisfied due to the diagonally dominant property. In the cases of the finite element discretization, each equation is associated with a basis function and the variables are the coefficients of the solution. To maximize the norm $\|J_{11}(u)\|_1$, one should choose the eliminated variables such that the eliminated equations and the eliminated variables are associated with the same finite element basis functions.

3.2. Inexact nonlinear elimination. In this subsection, we present a basic nonlinear solver: inexact Newton method (IN) [9, 11]. After that, we propose a nonlinearity checking scheme to detect the eliminated equations and then embed the nonlinear elimination into IN, which is briefly described here. Suppose u^k is the current approximate solution, a new approximate solution u^{k+1} is computed through the following two steps

ALGORITHM 1 (IN).
Step 1: Find the inexact Newton direction p^k such that
$$\|F(u^k) + F'(u^k)p^k\| \leq \eta_k \|F(u^k)\|,$$

Step 2: Compute the new approximate solution with suitable damping coefficient λ^k

$$u^{k+1} = u^k + \lambda^k p^k.$$

Here $\eta_k \in [0, 1)$ is a scalar that determines how accurately the Jacobian system needs to be solved, and λ^k is another scalar that determines how far one should go in the selected direction.

The nonlinear elimination substitutes the current guess u^k by $\bar{u}^k$, which is obtained by solving a nonlinear subproblem. Next we construct the subproblem. Let

$$S = \{1, \cdots, n\}$$

be an index set; i.e., one integer for each unknown u_i and residual F_i. Here we abuse the notation of subscript to indicate a component of the vectors. The following index set collects the degrees of freedom (d.o.f.) with large residual components:

$$S_b := \{j \in S \mid |F_j(u^k)| > \rho_{res}\|F(u^k)\|_\infty\}.$$

Following a trick of the Schwarz method, we extend S_b to S_b^δ by adding the neighboring d.o.f. with overlapping δ to S_b. The resulting subspace is denoted by

$$V_b^\delta = \{v \mid v = (v_1, \cdots, v_n)^T \in \mathrm{R}^n, v_k = 0, \text{ if } k \notin S_b^\delta\}.$$

The corresponding restriction operator is denoted by $R_b^\delta \in \mathrm{R}^{n\times n}$, whose kth column is either zero if $k \notin S_b^\delta$ or the kth column of the indentity matrix $I_{n\times n}$.

Given an approximate solution u^k and an index set S_b^δ, the nonlinear elimination algorithm finds the correction by approximately solving $u_b \in V_b^\delta$,

$$F_b^\delta(u_b) := R_b^\delta F(u_b + u^k) = 0. \tag{3.18}$$

The new approximate solution is obtained as $\bar{u}^k = u_b + u^k$. It is easy to see that the Jacobian of (3.18) is $J_b^\delta(u_b) = R_b^\delta J(u_b + u)(R_b^\delta)^T$, Here $J = F'$.We summarize the nonlinear elimination preconditioned inexact Newton method (NEPIN) as follows:

ALGORITHM 2 (NEPIN).

Step 1 Perform the nonlinearity checking:

1.1 If the reduction rate $\frac{\|F(u^k)\|}{\|F(\bar{u}^{k-1})\|} \le \rho_{rdt}$, *set* $\bar{u}^k = u^k$ *and go to Step 3.*

1.2 Find the eliminated d.o.f. and construct the index set S_b^δ.

1.3 If $\#(S_b^\delta) < \rho_{size} n$, *go to Step 2. Otherwise, set* $\bar{u}^k = u^k$ *and go to Step 3.*

Step 2 Compute the correction $u_b^\delta \in V_b^\delta$ *by solving the subproblem approximately*

$$F_b^\delta(u_b^\delta) := R_b^\delta F(u_b^\delta + u^k) = 0,$$

with a tolerance $\mathrm{tol} = \max(\gamma_a, \gamma_r\|R_b^\delta F(u^k)\|)$. *If* $\|F(u_b^\delta + u^k)\| < \|F(u^k)\|$, *accept the correction and update* $\bar{u}^k \leftarrow u_b^\delta + u^k$. *Go to Step 3.*

Step 3 Compute the new approximate solution u^{k+1} *by one step of IN for the original nonlinear problem*

$$F(u) = 0$$

with the current guess $\bar{u}^k$. *If the global convergent condition is satisfied, stop. Otherwise, go to Step 1.*

In the nonlinearity checking step, there are five tolerance parameters: ρ_{damp} and ρ_{rdt} are the tolerances to evaluate the local nonlinearity, ρ_{res} and δ are the tolerances to select the eliminated equations, and ρ_{size} is the tolerance to limit the size of the subproblem.

In nonlinear elimination step, we only accept the correction by nonlinear elimination if the resulting residual norm is smaller. This is based on Lemma 3.2, which tells us that an effective nonlinear elimination should reduce the global residual. This requirement actually is very strong. Whereas, according to our numerical tests, it can be satisfied if a good initial guess is provided or the tolerance δ is appropriately set.

4. Numerical results and discussion. In this section, we present some numerical results for solving the nonlinear variational problem (2.3). We first validate our algorithm and implementation. Then we compare the performance of the classical inexact Newton method with our new algorithm. In the end, we discuss the robustness of the nonlinear elimination. Our 3D geometry is built through extruding the cross-section in Fig. 2.1 by 2mm. A pressure of up to 24kPa ($\approx$ 180mmHg) is applied to the interior of the arterial segment, which is the upper range of the physiological blood pressure. The discretization for hyperelasticity and the nonlinear solvers described in the previous sections are implemented by using FEniCS [16] and PETSc [1], respectively.

In all tests, the stopping criterion for the outer nonlinear solvers is

$$\|F(u^k)\| \leq \max(1\text{e}{-10}, 1\text{e}{-6}\|F(u^0)\|).$$

The backtracking line search strategy is used to determine the maximum amount to move along the Newton direction. The right-preconditioned GMRES is used for solving the global Jacobian system with zero initial guess and the restart is set to 200. The stopping criterion for the linear solvers is

$$\|F(u^k) + F'(u^k)p^k\| \leq \max(1\text{e}{-10}, 1\text{e}{-5}\|F(u^k)\|).$$

The restricted additive Schwarz preconditioner is used with overlapping $\delta = 3$ and LU solvers for the subdomain problems.

4.1. Validation of algorithm and software. It is hard to construct an analytic solution for the nonlinear variational problems. One way to validate the result is to observe the mesh convergence of the numerical solutions. We generate four tetrahedral meshes for the arterial segment, denoting by M_1, M_2, M_3, and M_4. The number of degrees of freedom defined on these meshes are 10080, 21693, 101046 and 653601 respectively. Because of the curved boundary of the artery, the domains occupied by these meshes are a little bit different. We plot the numerical solutions of displacement in Fig. 4.1 for the case of the simple boundary load and the von Mises stresses in Fig. 4.4 for the case of follower boundary load. The deformation driven by the simple pressure load is bigger then that driven by the follower pressure load, but their distributions and the stresses are similar. It is clear that the computed solutions converge as the mesh is refined. Moreover, we compare the numerical solutions computed by IN and NEPIN. They are almost indistinguishable.

4.2. A comparison of IN and NEPIN. We use different initial guesses to compare the performance of IN and NEPIN. The number of global Newton iterations are summarized in Table 4.1. In these two tables, we denote $\bar{u}_{h_i}$ as the numerical solution of M_i driven by the simple pressure load, and u_{h_i} for that driven by the

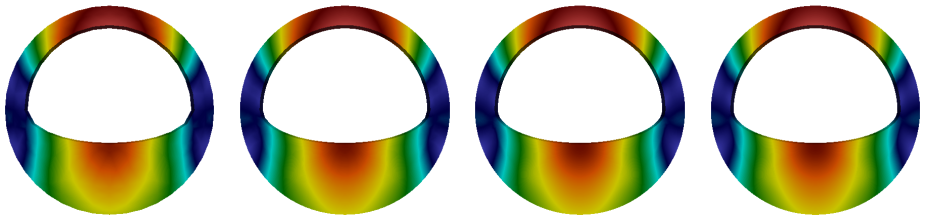

Fig. 4.1: Numerical solutions of the displacement corresponding to meshes M_1, M_2, M_3, M_4 from left to right (simple boundary load)

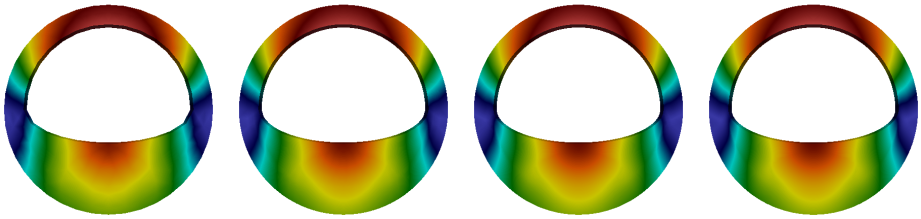

Fig. 4.2: Numerical solutions of the displacement corresponding to meshes M_1, M_2, M_3, M_4 from left to right (follower boundary load)

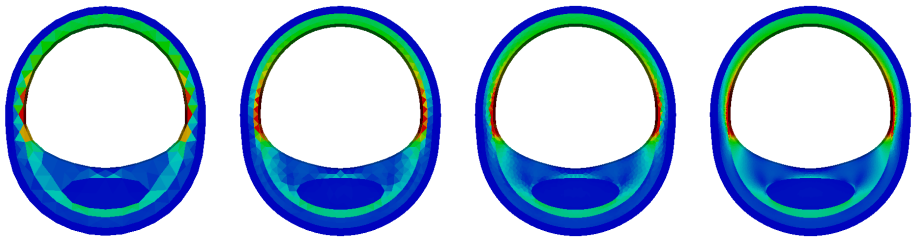

Fig. 4.3: von Mises stresses on the deformed configurations corresponding to meshes M_1, M_2, M_3, M_4 from left to right (simple pressure load)

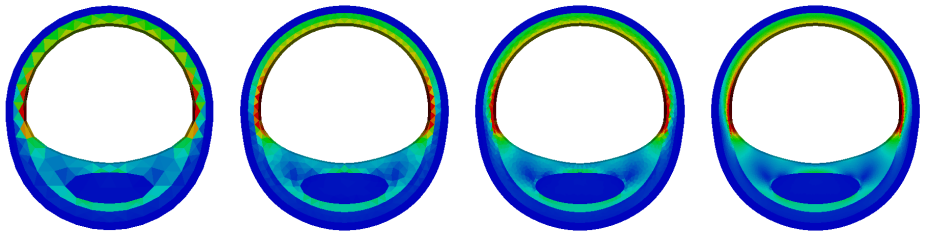

Fig. 4.4: von Mises stresses on the deformed configurations corresponding to meshes M_1, M_2, M_3, M_4 from left to right (follower boundary load)

Method	IN				NEPIN			
Initial guess\mesh	M_1	M_2	M_3	M_4	M_1	M_2	M_3	M_4
0	104	121	109	93	38	49	58	92
$I_{h_1}^{h_i}\bar{u}_{h_1}$		100	94	F		21	24	F
$I_{h_2}^{h_i}\bar{u}_{h_2}$			106	F			21	23
$I_{h_3}^{h_i}\bar{u}_{h_3}$				F				22

Table 4.1: The number of global Newton iterations with different initial guesses (simple pressure load)

Method	IN				NEPIN			
Initial guess\Mesh	M_1	M_2	M_3	M_4	M_1	M_2	M_3	M_4
0	F	F	F	F	F	F	F	F
$I_{h_1}^{h_i}\bar{u}_{h_1}$	28	88	144	F	23	28	30	69
$I_{h_1}^{h_i}u_{h_1}$		87	97	F		20	21	F
$I_{h_2}^{h_i}u_{h_2}$			42	F			14	33
$I_{h_3}^{h_i}u_{h_3}$				F				17

Table 4.2: The number of global Newton iterations with different initial guesses (follower pressure load)

follower pressure load. The letter F indicates that the iteration does not converge in 200 steps. We also denote the nodal interpolation operator by $I_{h_i}^{h_j}$, which prolongates the numerical solutions from M_i to M_j. Note that some nodal values are computed via extrapolation since some nodes of the fine mesh are outside the domain occupied by the coarse mesh. In the context of quasi-incompressible linear elasticity, the nodal interpolation is unstable since it does not preserve the volume. But in our numerical tests for quasi-incompressible hyperelasticity, the combination of the nonlinear elimination with the nodal interpolation works well.

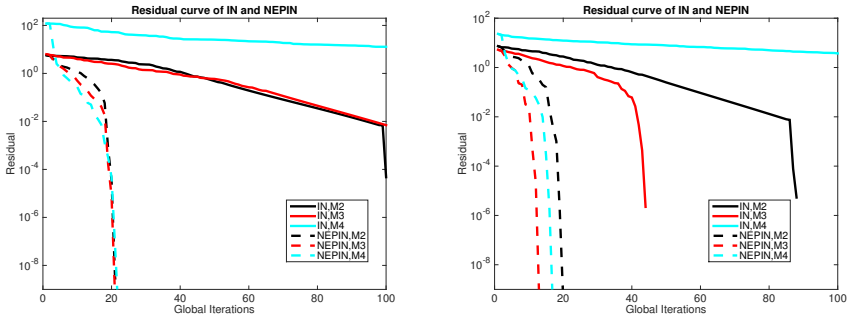

Fig. 4.5: Histories of IN and NEPIN (left: simple pressure load , right: follower pressure load)

The first thing we observe from Table 4.1-4.2 is that NEPIN always converges

faster than IN while using the same initial guess and the same mesh. For the zero initial guess, the performance of nonlinear elimination is not good enough. Actually, both methods with zero initial guess for the case of the follower load fail. When the zero initial guess is too far from the solution, the local nonlinear elimination does not help much for the global Newton iteration. However, once an approximate initial guess is provided, the performance of nonlinear elimination is prominent. Note that IN with the same initial guess still suffers from slow convergence. Fig. 4.5 shows the histories of the residual of IN and NEPIN starting from the best available initial guesses. Namely, the initial guess for M_i is interpolated from the numerical solution of M_{i-1}. The convergence of NEPIN is almost uniform for all meshes.

Mesh		M_2			M_3			M_4		
$\delta \backslash \rho_{res}$		0.7	0.8	0.9	0.7	0.8	0.9	0.7	0.8	0.9
0	GN	25	23	21	30	34	47	31	52	50
	ANE	$\frac{21}{10}$	$\frac{22}{14}$	$\frac{25}{17}$	$\frac{68}{17}$	$\frac{57}{29}$	$\frac{77}{42}$	$\frac{60}{26}$	$\frac{118}{47}$	$\frac{108}{45}$
	pct.	3.9%	4.4%	3.0%	3.3%	4.3%	0.8%	0.8%	0.5%	0.2%
1	GN	25	32	30	24	21	26	24	28	34
	ANE	$\frac{42}{5}$	$\frac{30}{4}$	$\frac{71}{10}$	$\frac{99}{12}$	$\frac{133}{12}$	$\frac{108}{21}$	$\frac{119}{16}$	$\frac{135}{22}$	$\frac{175}{26}$
	pct.	4.9%	4.9%	4.9%	4.0%	4.1%	4.1%	3.6%	1.9%	0.6%
2	GN	100	69	56	29	30	22	26	21	30
	ANE	$\frac{0}{0}$	$\frac{8}{1}$	$\frac{50}{3}$	$\frac{161}{13}$	$\frac{131}{12}$	$\frac{117}{12}$	$\frac{110}{12}$	$\frac{128}{14}$	$\frac{199}{23}$
	pct.	0%	4.5%	4.9%	4.4%	3.6%	4.8%	3.0%	2.7%	1.2%

Table 4.3: The performance of NEPIN using different tolerances δ and ρ_{res}, (GN: the number of global Newton iterations, ANE: $\frac{\text{the total Newton iterations for NE}}{\text{the number of NE}}$, pct.: the maximum percentage of the eliminated equations)

Mesh$\backslash\gamma_r$	1e−1		1e−2		1e−4		one step	
	GN	ANE	GN	ANE	GN	ANE	GN	ANE
M_2	23	$\frac{25}{17}$	25	$\frac{80}{18}$	23	$\frac{66}{17}$	23	$\frac{21}{21}$
M_3	24	$\frac{121}{14}$	25	$\frac{203}{15}$	24	$\frac{251}{15}$	70	$\frac{44}{44}$
M_4	24	$\frac{180}{17}$	19	$\frac{202}{12}$	19	$\frac{301}{15}$	98	$\frac{82}{82}$

Table 4.4: The performance of NEPIN using different tolerance γ_r for subproblems

4.3. The effect of the tolerances in NEPIN. We set $\rho_{damp} = 0.1, \rho_{rdt} = 0.7$ to evaluate the local nonlinearity and set $\rho_{size} = 5\%$ to limit the subproblem size. There are two main factors impacting the performance of NEPIN: how to choose the equations to eliminate and how approximately the subproblems need to solve.

The index set S_b^δ of the eliminated equations is determined by two tolerance ρ_{res} and δ. Table 4.3 lists the convergence results of NEPIN for different setting for ρ_{res} and δ. The performance of NEPIN is not sensitive to the choice of ρ_{res}. In the middle row of the table, where $\delta = 1$, the number of global Newton iterations varies from 20 to 34, which indicates the convergence of NEPIN is almost uniform with respective to the mesh size. For coarse meshes, δ should not be larger than 1, otherwise the size of S_n^δ, i.e. the number of equations to eliminate, is too large. For fine meshes, δ

should be larger than 0, otherwise the preconditioning effect of NEPIN is too weak. Another satisfying observation from the table is that the percentage of the equations to eliminate decreases as the mesh is refined. The average Newton iterations for solving one subproblem is 5, while we set the relative tolerance $\gamma_r = 0.1$ for the subproblems. Table 4.4 shows the performance of NEPIN for different γ_r. The number of global Newton iterations is not sensitive to this tolerance. A very loose tolerance, say 0.1 is sufficient, which is the same to the results in [12].

5. Conclusions. The main contribution of this paper is to present a detailed analysis on the preconditioning effect of nonlinear elimination and to apply the proposed method to 3D heterogenous hyperelastic problems. In theory, we prove that the exact nonlinear elimination is also able to increase the step length during the line search step of IN and then accelerates the convergence of Newton iterations. In numerical computation, we propose a robust strategy to detect the equations causing the nonlinear stagnation. We also find two effective tricks to ease the thrashing phenomenon of nonlinear elimination: using an initial guess interpolated from a coarse level solution and extending the eliminating index set by adding the neighboring d.o.f.. As future work, we will consider other arterial wall problems with patient-specific geometry and the parallel performance of the algorithm.

REFERENCES

[1] S. Balay, S. Abhyankar, M. F. Adams, J. Brown, P. Brune, K. Buschelman, L. Dalcin, V. Eijkhout, W. D. Gropp, D. Kaushik, M. G. Knepley, L. C. McInnes, K. Rupp, B. F. Smith, S. Zampini, H. Zhang, and H. Zhang, *PETSc users manual*, Tech. Report ANL-95/11 - Revision 3.7, Argonne National Laboratory, 2018.

[2] J. M. Ball, *Convexity conditions and existence theorems in nonlinear elasticity*, Arch. for Ration. Mech. Analysis, 63 (1976), pp. 337–403.

[3] D. Balzani, S. Deparis, S. Fausten, D. Forti, A. Heinlein, A. Klawonn, A. Quarteroni, O. Rheinbach, and J. Schröder, *Numerical modeling of fluid–structure interaction in arteries with anisotropic polyconvex hyperelastic and anisotropic viscoelastic material models at finite strains*, Int. J. Num. Methods Biomed. Eng., (2015).

[4] D. Balzani, P. Neff, J. Schröder, and G. A. Holzapfel, *A polyconvex framework for soft biological tissues. Adjustment to experimental data*, Int. J. Solids Struct., 43 (2006), pp. 6052–6070.

[5] Y. Bazilevs, K. Takizawa, and T. E. Tezduyar, *Computational Fluid-structure Interaction: Methods and Applications*, John Wiley & Sons, 2013.

[6] D. Brands, A. Klawonn, O. Rheinbach, and J. Schröder, *Modelling and convergence in arterial wall simulations using a parallel FETI solution strategy*, Comput. Methods Biomech. Biomed. Eng., 11 (2008), pp. 569–583.

[7] X.-C. Cai and D. E. Keyes, *Nonlinearly preconditioned inexact newton algorithms*, SIAM J. Sci. Comput., 24 (2002), pp. 183–200.

[8] X.-C. Cai and X. Li, *Inexact Newton methods with restricted additive Schwarz based nonlinear elimination for problems with high local nonlinearity*, SIAM J. Sci. Comput., 33 (2011), pp. 746–762.

[9] R. S. Dembo, S. C. Eisenstat, and T. Steihaug, *Inexact Newton methods*, SIAM J. Num. Anal. 19 (1982), pp. 400–408.

[10] P. Deuflhard, *Newton Methods for Nonlinear Problems: Affine Invariance and Adaptive Algorithms*, vol. 35, Springer Science & Business Media, 2011.

[11] S. C. Eisenstat and H. F. Walker, *Globally convergent inexact Newton methods*, SIAM J. Optim., 4 (1994), pp. 393–422.

[12] F.-N. Hwang, Y.-C. Su, and X.-C. Cai, *A parallel adaptive nonlinear elimination preconditioned inexact newton method for transonic full potential equation*, Computers & Fluids, 110 (2015), pp. 96–107.

[13] J. Huang, C. Yang, and X.-C. Cai, *A nonlinearly preconditioned inexact Newton algorithm for steady state lattice Boltzmann equations*, SIAM J. Sci. Comput., 38 (2016), pp. A1701–A1724.

[14] R. Knops and P. Ciarlet, *Mathematical Elasticity, Vol. 1. Three-dimensional Elasticity*, Bulletin of the AMS, 31 (1994), pp. 246–251.

[15] P. J. Lanzkron, D. J. Rose, and J. T. Wilkes, *An analysis of approximate nonlinear elimination*, SIAM J. Sci. Comput., 17 (1996), pp. 538–559.

[16] A. Logg, K.-A. Mardal, and G. Wells, *Automated Solution of Differential Equations by the Finite Element Method: The FEniCS Book*, vol. 84, Springer Science & Business Media, 2012.

[17] J. Schröder and P. Neff, *Invariant formulation of hyperelastic transverse isotropy based on polyconvex free energy functions*, Int. J. Solids Struct., 40 (2003), pp. 401–445.